Title: Fingerprinting Adiposity and Metabolic Function in the Brains of Overweight and Obese Humans

Authors: Michael C. Farruggia[a,b], Maria J. Van Kooten[b,c], Mary V. Burke[a,b], Dustin Scheinost[d,e,f], R. Todd Constable[a,d,g], Dana M. Small[a,b,h,i]

Affiliations:
[a]Interdepartmental Neuroscience Program, Yale University, 333 Cedar Street, New Haven, CT, U.S.
[b]Department of Psychiatry, Yale University School of Medicine, 300 George Street, New Haven, CT 06511, USA.
[c]University of Groningen, Faculty of Medical Sciences, Antonius Deusinglaan 1, 9713 AV Groningen, The Netherlands.
[d]Department Radiology and Biomedical Imaging, Yale University School of Medicine, New Haven, CT, United States.
[e]Department Statistics and Data Science, Yale University, New Haven, CT, United States.
[f]Child Study Center, Yale School of Medicine, New Haven, CT, United States.
[g]Department of Neurosurgery, Yale University School of Medicine, New Haven, CT, United States.
[h]Department of Psychology, Yale University, New Haven, CT, United States.
[i]fMEG Center, University of Tubingen, Tubingen, Germany.

Correspondence should be addressed to:
*Dana M Small, PhD
dana.small@yale.edu
(D.M.S.)
*Michael C Farruggia, MS
michael.farruggia@yale.edu
(M.C.F.)
1 Church Street, Suite 6a
New Haven, CT 06510
Phone: (954) 325-2660

Other Contact Information:
Maria J. Van Kooten: +31683660266; m.j.van.kooten@umcg.nl; 1 Church Street, Suite 6a, New Haven, CT, 06510
Mary V. Burke: 845-705-6890; mary.burke@yale.edu; 1 Church Street, Suite 6a, New Haven, CT, 06510
Dustin Scheinost: 203-824-2017; dustin.scheinost@yale.edu; 300 Cedar Street, Rm. N131, New Haven, CT, 06519
R. Todd Constable: 203-737-2768; todd.constable@yale.edu; 300 Cedar Street, Rm. N130, New Haven, CT, 06519

Note: With the exception of its pre-print on bioRxiv, none of the material has been published or is under consideration elsewhere, including the Internet.

Abstract: The brain plays a central role in the pathophysiology of obesity. Connectome-based Predictive Modeling (CPM) is a newly developed, data-driven approach that exploits whole-brain functional connectivity to predict a behavior or trait that varies across individuals. We used CPM to determine whether brain "fingerprints" evoked during milkshake consumption could be isolated for common measures of adiposity in 67 overweight and obese adults. We found that a CPM could be identified for waist circumference, but not percent body fat or BMI, the most frequently used measures to assess brain correlates of obesity. In an exploratory analysis, we were also able to derive a largely distinct CPM predicting fasting blood insulin. These findings demonstrate that brain network patterns are more tightly coupled to waist circumference than BMI or percent body fat and that adiposity and glucose tolerance are associated with distinct maps, pointing to dissociable central pathophysiological phenotypes for obesity and diabetes.

Keywords:

Adiposity; metabolism; waist circumference; insulin; fMRI; functional connectivity; predictive modeling; obesity

61 **Introduction**

62 Obesity is a neurobehavioral disorder resulting from a biologically vulnerable brain that is highly
63 sensitive to its environment (*1*). Evidence for this derives from genome-wide association studies
64 (GWAS), demonstrating that genetic variants associated with obesity tend to affect brain
65 function. For example, high-risk variants in the FTO (fat mass and obesity associated) gene
66 predispose individuals to weighing on average 3kg more and increasing their obesity risk 1.67x
67 over those with low-risk variants (*2*, *3*). The FTO gene encodes the alpha-ketoglutarate-
68 dependent dioxygenase enzyme, a protein that is highly expressed in the human brain,
69 particularly in the hypothalamus and cerebellum as well as on dopamine receptors where it
70 influences reward learning (*4* - *6*). Hypotheses of FTO's action in the human brain suggest that it
71 may act to increase consumption of food and alter sensing of dietary macronutrient composition
72 (*7*). Since the discovery of FTO, additional GWAS have found another 97 BMI-associated SNPs
73 which encode for proteins that are significantly enriched in the human brain (*8*).
74 While the vast majority of evidence continues to point to the brain as integral in the
75 pathophysiology of obesity, none of the adiposity measures we have to quantify it or characterize
76 its extent are brain measures. Body mass index, or BMI, is the anthropometric measurement
77 commonly used to classify obesity, with individuals having a BMI ≥ 30 characterized as obese
78 (*9*). However, BMI as a measure of adiposity is often criticized for being an inaccurate reflection
79 of fat mass, in particular in Asians and in athletes (*10*, *11*). Body fat percentage alone has also
80 been criticized as an inaccurate predictor of negative health outcomes, as regional distribution of
81 fat in the body influences risk for negative health consequences. For example, women with
82 predominantly upper body adipose tissue are more likely to have diabetic glucose tolerance
83 results and higher fasting plasma triglycerides than those with predominantly lower body adipose

84 tissue (*12*). More recent studies have found that distribution of adipose tissue, particularly in the
85 thighs, is inversely correlated with metabolic syndrome in obesity (*13*).
86 Ultimately, if obesity is a neurobehavioral disorder resulting from a vulnerable brain interacting
87 with an obesogenic environment, the most informative adiposity measures should be predicted
88 by brain function to some extent. Further, if an adiposity measure can be reliably predicted using
89 features of brain function in a cross-validated framework, it follows that these features may
90 represent a generalizable index of adiposity. Thus, not only is it important that we are able to
91 determine which adiposity measure is best predicted by whole-brain functional connectivity, but
92 it also imperative to determine which anatomical regions (i.e. nodes) and which connections
93 among them (i.e. edges) are influencing our predictive power.
94 With this in mind, we set out to determine which commonly-used adiposity measures, including
95 BMI, body fat %, waist size, body weight, and waist/hip ratio, could be predicted by whole-brain
96 function connectivity. To accomplish this, we use connectome-based predictive modeling
97 (CPM), a data-driven approach that builds predictive models of brain-behavior relationships
98 using connectivity data in a cross-validated framework (*14*, *15*). More specifically, CPM exploits
99 individual variation in whole-brain functional connectivity to predict a behavior or trait that
100 varies across individuals in a leave-one-out procedure. CPM has been used to identify brain
101 "fingerprints" (*14*) as well as to predict personality traits (*16*), creative ability (*17*), and sustained
102 attention (*18*). Here we used this technique to ask whether a predictive CPM could be identified
103 for our different adiposity measures. As an exploratory aim, we also tested whether a CPM could
104 be found for measures of glucose tolerance.
105
106 **Results**

107 **CPM predicts individual differences in waist circumference**

108 Of all measures, including BMI, body fat %, waist size, body weight, and waist/hip ratio, we
109 found that CPM significantly predicts waist circumference (combined network, $r = 0.354$, $p =$
110 0.005) after applying Benjamini-Hochberg FDR correction for multiple tests (Fig. 1). Overall,
111 the combined model accounts for approximately 12.5% of the variance in the waist
112 circumference of a novel subject.

113 **Waist circumference CPM contains DMN, motor, visual, cerebellar, and subcortical**
114 **networks**

115 The combined model consists of edges whose strengths are positively (positive network) or
116 negatively (negative network) correlated with our variable of interest, waist circumference.
117 These edges can be visualized as connections among nodes assigned to one of ten bilateral brain
118 regions (Fig. 2A), or as the density of edges among ten canonical networks normalized by
119 network size (Fig. 2B). Brain regions include Prefrontal, Motor, Insula, Parietal, Temporal,
120 Occipital, Limbic, Cerebellum, Subcortical, and Brainstem. We operationally define our high
121 degree nodes as the top N nodes that occur before multiple degree repetitions. High degree nodes
122 (degree ≥ 9), or nodes with the highest number of connections for the waist circumference CPM
123 were found in prefrontal, parietal, limbic, cerebellar, subcortical, and temporal regions (Fig. 2A,
124 *see also 5A*). AAL labels for these regions include left inferior frontal gyrus, left postcentral
125 gyrus, left amygdala, left culmen of cerebellum, right putamen and right fusiform gyrus,
126 respectively (Table 1).

127 Canonical networks emphasize different functional properties of the human brain and consist of
128 medial frontal (MF), frontoparietal (FP), default mode (DM), motor (MO), visual 1 (V1), visual
129 2 (V2), visual association (VA), cingulo-opercular (CO), subcortical (SC), and cerebellum (CE)

130 networks (*19*, *20*). The highest proportion of edges, that is, the edges used most in prediction for
131 the positive network exist between DM-V2, MO-CE, V2-VA, and CO-SC. In the negative
132 network, these are between DM-SC, MO-V2, MO-V1, V1-SC, VA-VA, and CE-CE (Fig. 2B).

133 **Exploratory analysis: CPM predicts individual differences in fasting insulin**

134 Due to the large scope of the dataset, we were able to conduct a post-hoc exploratory analysis of
135 metabolic markers to examine convergence or divergence of predictive networks as they relate to
136 the waist circumference CPM. For this analysis, we analyzed additional bloods data until we had
137 a complete metabolic panel from all 59 of 67 subjects. Fasting glucose, fasting insulin, and
138 HOMA-IR were input into CPM as our measures of interest. CPM was able to predict fasting
139 insulin ($p < 0.05$, uncorrected; Fig. 3A) but not fasting glucose or HOMA-IR, accounting for
140 approximately 7% of the variance in a novel individual's fasting insulin levels. Positive and
141 negative predictive networks for fasting insulin are notably sparser than those for waist
142 circumference (Fig. 3B). High degree nodes (degree ≥ 6) for these networks were found in
143 cerebellar (left crus and right lobule VIIB), temporal (left superior temporal pole and right
144 fusiform), and limbic (right posterior cingulate gyrus) regions (Fig. 3B, *see also 5B, Table 2*). In
145 the positive network, a high density of edges exists between MF-CE, DM-V2, MO-CE, V2-CE,
146 and V2-SC (Fig. 3C). In the negative network, these exist between MF-MF, FP-VA, FP-V1,
147 DM-CE, DM-SC, V1-SC, V1-V2, VA-CO, CO-CE, and SC-SC (Fig. 3C).

148 **Waist circumference and fasting insulin CPMs are separable**

149 To examine convergence and divergence of predictive networks, we subtracted the number of
150 negative edges from the number of positive edges between each canonical network and plotted
151 the resultant degree of polarity (Fig. 4A-B). For example, networks can have mostly positive or
152 negative edges connecting them (i.e. polarity), or an even distribution of positive and negative

153 edges (i.e. apolarity). Indeed, this technique demonstrates the degree to which positive or
154 negative edges are used in prediction and can help ascertain common or uncommon
155 neurobiological correlates between fasting insulin and waist circumference. The predictive
156 network for waist size shows a large degree of polarity (Fig. 4A), while the relative sparsity of
157 the predictive network for insulin is visible and there is notable apolarity particularly among
158 visual networks (Fig. 4B). Predictive networks for insulin and waist size are on average
159 dissimilar. Of the 55 network pairs, 26 network pairs (47%) exhibited similar degrees of polarity
160 between the waist circumference and insulin predictive networks. Most notably, patterns of
161 connectivity within cerebellar and subcortical networks showed the most similar patterns of
162 polarity between waist circumference and fasting insulin predictive networks (Fig. 4). In contrast
163 their polarity differs most in medial-frontal, frontoparietal, default mode, motor, visual, and
164 cingulo-opercular networks. To aid in comparison, we plotted the spatial extent of the top 10%
165 highest-degree predictive nodes for each network (Fig. 5A-B, Tables 1 & 2). Only nine of the top
166 10% of nodes (27 total) in each CPM are shared among each other, those being centered in left
167 posterior cingulate gyrus (node 227), right fusiform (59), right and left superior temporal pole
168 (92 and 188), left cerebellum (255), left and right lobule III of cerebellum (251 and 103), left
169 crus II of cerebellum (242), and midbrain (132). The 18 nodes (66%) that differ are depicted in
170 Fig. 6A-B.

171 **The role of subject motion**

172 We used frame-to-frame displacement (FTF) as a gross measure of head motion (*21*). FTF was
173 calculated for each run in each subject and averaged across runs. FTF significantly correlated
174 with waist size ($R^2 = 0.199$, $p < 0.001$), BMI ($R^2 = 0.115$, $p < 0.01$), body weight ($R^2 = 0.132$, p
175 < 0.01), waist/hip ratio ($R^2 = 0.103$, $p < 0.01$), and BF% ($R^2 = 0.107$, $p < 0.01$). FTF was notably

176 not correlated with fasting glucose (r = 0.05, p = 0.68), fasting insulin (r = 0.15, p = 0.25), or
177 HOMA-IR (r = 0.15, p = 0.27). While a correlation between any of our adiposity measures and
178 FTF suggests that motion should be accounted for using partial Pearson correlation, recent
179 evidence suggests that in-scanner head motion is heritable and phenotypically correlated with
180 BMI (*22*). Indeed, if head motion and adiposity contain shared genetic influences, then
181 controlling for motion in CPM would unnecessarily reduce its predictive power in this instance.
182 Instead we corrected for motion during preprocessing (see Methods) and report results following
183 partial Pearson correlation for mean FTF subject (see Supplementary Table 2). Of note, CPMs
184 for both waist circumference and insulin were both significant, but did not survive FDR
185 correction when motion is included as a covariate.
186
187 **Discussion**
188 Our experiment produced several novel findings. First, we determined, using a data-driven
189 approach, that waist circumference could be predicted by whole-brain functional connectivity. In
190 particular, with CPM we can account for approximately 12.5% of the variance in this measure in
191 a novel individual. Notably, we could not predict BMI, the most commonly used measure to
192 define obesity, or other adiposity measures, such as body fat %, body weight, and waist/hip ratio.
193 Second, we found that a metabolic marker, fasting insulin, could be predicted from whole-brain
194 functional connectivity and that this predictive network was distinct from that of waist
195 circumference.
196 There is long-standing controversy regarding the optimal method to quantify adiposity. We
197 assert that, not only is it important to use a measure that captures an individual's risk for

198 morbidity and mortality, but it is equally important to capture obesity's underpinnings as a
199 neurobehavioral disorder. Waist circumference does both.
200 This proposal is consistent with a number of recent findings. Waist circumference has better
201 discriminatory capability for type 2 diabetes than either BMI or body adiposity index [BAI,
202 calculated as (hip circumference)/((height)$^{1.5}$)–18] in a northern Iranian population (*23*, *24*). A
203 systematic review found that waist circumference performed 3% better than BMI in
204 discriminating adults with hypertension, T2D, metabolic syndrome, dyslipidaemia, and general
205 cardiovascular outcomes (*25*). A meta-analysis of some 259,200 individuals found that high
206 waist circumference is a better predictor than high BMI for the development of diabetes across
207 all ethnicities tested and for the development of hypertension among Hispanics/Latinos in
208 particular (*26*). Additional evidence suggests that individuals who are classified as obese by
209 waist circumference have a greater risk for all-cause and cardiovascular disease-related death
210 than individuals who are classified as obese by BMI (*27*). In a separate cohort of 2266
211 hypertensive patients, waist circumference was able to predict the development of coronary
212 artery disease, while other measures of adiposity such as BMI and waist/hip ratio had no
213 independent prognostic value (*28*).
214 Although most neuroimaging studies use BMI to assess neural correlates of obesity, when waist
215 circumference is pitted against BMI, stronger and more extensive correlations are often found.
216 For example, waist circumference, is a better predictor of local gray matter volume
217 (*29*, *30*) and brain response to food cues (*31 – 33*). The current study confirms and extends these
218 findings by using functional connectivity and a whole-brain data-driven approach to show that
219 brain measures not only correlate most strongly with waist circumference, but also are able to

220 predict waist circumference. This indicates that this neural measure may act as a biomarker for
221 the measure of adiposity that best predicts obesity-related health outcomes (*34*).
222 More specifically, high-degree nodes for the waist circumference CPM were located in left
223 inferior frontal gyrus, left postcentral gyrus, left amygdala, the left culmen of the cerebellum,
224 right putamen, and right fusiform gyrus (Fig. 5A). Enhanced responses to food-related stimuli
225 can be found in many of these regions and responses in some regions have been associated with
226 weight gain (*35*, *36*). However, in these instances the relationship is correlative. For example,
227 amygdala response to food related stimuli when sated, but not hungry, correlates with 12-month
228 weight gain (*37*). This suggests that amygdala responsivity to food cues in the absence of hunger
229 is predictive of overeating and weight gain, but it is not a direct test of the hypothesis because the
230 amygdala response could be epiphenomenal. Likewise, response in the right putamen, during
231 milkshake consumption is predictive of weight change with direction depending upon genotype
232 (*38*). The current results go beyond these findings. CPM presents as a strength its cross-validated
233 framework based on data-driven model optimization. Here we were able to identify brain
234 features that predict and therefore may constitute a neural index of waist circumference.
235 This result raises the question as to how the CPM we have identified contributes to the
236 development of increased waist circumference and conversely, how and why waist
237 circumference specifically influences the identified brain "fingerprint". Notably, although waist
238 circumference is the best adiposity predictor of glucose control, inspection of the anatomy of the
239 CPMs identified for waist circumference and fasting insulin, a marker of insulin resistance,
240 reveals that they are largely distinct (Fig. 5, 6) (*39 – 41*). In particular, the CPMs for waist
241 circumference and fasting insulin showed minimal overlap in the highest degree nodes. This
242 suggests there are distinct neuropathophysiological features. The distinction between the CPMs

243 is best captured by their relative polarity, or the number of positive versus negative edges
244 between networks. The cerebellar and subcortical networks show similar patterns of connectivity
245 while patterns in medial-frontal, frontoparietal, default mode, motor, visual, and cingulo-
246 opercular networks largely differ. Overlap between cerebellar and subcortical networks for
247 adiposity and metabolic dysfunction suggests that these regions may play an integral role in the
248 pathophysiology of obesity. These observations support future efforts to uncover the link
249 between the distinct networks and their contributions to the causes and consequences of obesity.
250 Our findings also have clinical implications. One important application of neuroimaging in
251 clinical practice, is to enable the prediction of clinical outcomes using brain structure, activity, or
252 connectivity (*42*). Previous methods in predicting brain-behavior relationships tended to be
253 correlational, and thus would overfit to data and fail to generalize to novel individuals (*15*). As
254 indicated above, CPM presents as a strength its cross-validated framework, which suggests that
255 the predictive features for waist circumference and fasting insulin are generalizable within novel
256 subjects in this dataset. In other words, it is a window into the brain features that contribute to
257 predicting adiposity and metabolic outcomes and as such may constitute biomarkers to index risk
258 or the efficacy of therapeutic interventions.
259 Further, to apply such a finding to clinical practice, network-based prediction models of obesity
260 must be shown to generalize across samples, populations, and experimental settings (*42*). A
261 promising avenue to then implement CPM as a tool for clinical use is to use real-time fMRI
262 biofeedback to change connectivity patterns or activation profiles within predictive networks
263 across subjects. Similar approaches have been successfully used in previous studies, namely
264 those attempting to alleviate contamination anxiety, enhance emotion regulation capabilities, and
265 mitigate auditory verbal hallucinations in schizophrenia, among others (*43* – 45). Another

266 approach, similar to that of Rosenberg et al., 2016 (*46*), is to treat overweight and obesity using a
267 particular intervention and observe how the predictive networks change. We predict that more
268 efficacious treatments will reduce network strength within networks that predict high waist
269 circumference and fasting insulin, and increase the strength of antithetical networks. Recent
270 work suggests that networks obtained using CPM can predict abstinence during treatment for
271 cocaine dependence (*47*). If the obtained CPMs are relevant to the pathophysiology of obesity, it
272 is thus possible that they may predict weight loss during an intervention, which would be useful
273 for obese individuals seeking treatment. Finally, not only is waist circumference better than BMI
274 and other adiposity measures at predicting a variety of adverse health-related outcomes, but it is
275 also better predicted from whole-brain functional connectivity using CPM. This suggests that
276 including waist circumference as a measure of interest in a clinical setting is imperative to
277 accurately quantify the extent and progression of obesity.

278 **Limitations and future directions**

279 This study has a number of limitations to address. First, the sample size was relatively limited for
280 a study implementing CPM. It is quite possible that with more data we would be able to build a
281 more informative predictive model. Second, we only include overweight and obese individuals in
282 our dataset due to the nature and design of the longitudinal study for which this data was
283 originally collected. It is thus possible that these CPMs for waist circumference and fasting
284 insulin do not generalize to lean individuals. However, since biomarkers are needed to evaluate
285 therapeutic interventions it can be argued that an overweight/obese sample is most appropriate.
286 Third, because the study design was not specifically optimized for use in this analysis, it remains
287 to be seen whether inclusion of tasteless blocks reduced our predictive power. Tasteless may be
288 more similar to a classic rest condition than milkshake. Across all studies implementing CPM,

289 resting state is least able to maximize detection of individual differences (*19*). Fourth, we did not
290 use DEXA or whole-body MRI, which are considered the optimal measurement devices to
291 determine adiposity (*48*). Although, waist circumference and fasting insulin are more practical
292 measures, future work should validate our observations using the gold standard measures.
293 Finally, longitudinal studies are necessary to determine whether the obtained predictive networks
294 arise as a cause or consequence of increased fasting insulin and waist circumference.

295 **Conclusions**

296 Our analyses reveal that by characterizing whole brain connectivity during consumption of a
297 palatable energy-dense milkshake it is possible to predict an individual's waist circumference but
298 not BMI or percent body fat. This finding suggests that waist circumference is the phenotypic
299 marker of obesity that is most closely related to brain function during food consumption.
300 However, whether this brain biomarker is a cause or a consequence of waist size is unknown. We
301 were also able to predict fasting insulin but not glucose or HOMA-IR. Notably, although fasting
302 insulin reflects insulin resistance (*49*) and waist circumference has been shown to correlate with
303 insulin resistance, the CPMs predictive of waist circumference and fasting insulin were largely
304 distinct.

305

306 **Materials and Methods**

307 **Participants**

308 We recruited 100 overweight and obese individuals using media, flyer advertisements, and the
309 Yale Center for Clinical Investigation Help Us Discover database. Subjects were recruited to
310 participate in an ongoing clinical trial (NCT 01976156), but all related fMRI scans occurred at
311 baseline prior to any experimental manipulations. We screened participants via phone or online

312 to ensure they met the following criteria: right-handed, English-speaking, 18-45 years of age,
313 body mass index (BMI) of 25 or higher, nonsmokers, no psychiatric or neurological impairments
314 (including drug addiction, eating disorders), no obesity-related diseases such as type-2 diabetes,
315 no food allergies, no chemosensory impairments, and no MRI contraindications (pregnancy,
316 claustrophobia, metal implants, or prior head injury with loss of consciousness). In total, 67
317 participants (mean age = 30.7yrs, mean BMI = 33.3 ± 6.5) met these criteria and underwent
318 fMRI procedures. All participants provided written informed consent according to our protocol
319 that was approved by the Yale University School of Medicine Human Investigation Committee.

320 **Measures**

321 This study was part of a larger clinical trial (NCT 01976156). Below we outline the procedures
322 related to the baseline fMRI assessment, on which the analyses in this study are based.

323 **Physical Characteristics and Diet**

324 Participants arrived at the lab on the week of fMRI scanning for anthropometric measurements,
325 which included body weight, height, waist size, hip size, and adiposity. Adiposity, as described
326 by body fat percentage (BF%), was measured using air displacement plethysmography
327 (BodPod). Waist/Hip ratio and BMI (kg/cm^2) were subsequently calculated. Additional
328 participant characteristics are shown in Supplementary Table 1.

329 **Bloods**

330 Following an overnight fast of 10-12 hours, blood samples were collected from 59 out of 67
331 subjects. We were unable to collect bloods on eight subjects due to venipuncture difficulty.
332 Samples were collected, centrifuged immediately, and then frozen at either 80 °C (insulin) or 20
333 °C (glucose). Insulin protein concentrations were subsequently measured using a
334 radioimmunoassay kit (APLCO insulin ELISA Catalog #80-INSHU-E01.1, Salem, NH) and

335 plasma glucose concentrations were determined using a glucose oxidase analyzer (YSI
336 Incorporated, Yellow Springs, OH). Insulin sensitivity was calculated using the homeostasis
337 model of insulin resistance, or HOMA-IR, which is based on the following formula: [insulin
338 (mU/L) x glucose (mmol/L)]/22.5 (*50*).

339 **Image protocols**

340 All fMRI scans were scheduled during the week of blood draws, sometime between 8:00 AM
341 and 12:00 PM. Participants were instructed to arrive neither full nor hungry, and adherence to
342 these instructions were confirmed using internal state ratings. Structural and functional imaging
343 data were then collected on a Siemens 3.0T TIM Trio scanner at the Yale Magnetic Resonance
344 Research Center (MRRC), using the following scan parameters: high resolution T1-weighted
345 structural scan repetition time (TR) = 2530ms, echo time (TE) = 3.31ms, slice thickness = 1mm,
346 flip angle = 7°, field of view (FOV) = 256 x 256, 256 x 256 matrix, 176 slices; functional
347 milkshake run TR = 2000ms, TE = 20 ms, slice thickness = 3mm, flip angle = 80°, FOV = 220 x
348 220, matrix = 64 x 64, 40 contiguous slices.

349 fMRI scans consisted of two 9-minute runs that were divided into blocks of 4-8 cued
350 presentations of milkshake or tasteless solutions. These solutions were delivered in quantities of
351 0.5 mL over a 2s period followed by 7s to swallow. Different milkshake flavors were used to
352 reduce the possibility of stimulus habituation. After each block, participants rinsed their mouths
353 with 0.5mL of deionized water over a period of 2s and were given 3s to swallow. Blocks varied
354 in length from 36s to 72s and order of presentation was counterbalanced.

355 **Stimuli**

356 Milkshake stimuli were presented as two flavors, chocolate and strawberry. Chocolate
357 milkshakes were made by combining 12 fl oz of whole milk with equal parts Garelick Farms

358 Chug chocolate milkshake and Garelick Farms Chug cookies and cream milkshake. The
359 strawberry milkshake was made by combining 32 fl oz of whole milk with 6 fl oz of Hershey's
360 strawberry syrup. One subject did not like the taste of strawberry and instead was given a vanilla
361 milkshake created by mixing 32 fl oz whole milk with 6 fl oz of Eclipse vanilla syrup.
362 Milkshakes were presented in an interleaved manner to reduce the possibility of sensory
363 adaptation. Tasteless solutions were chosen individually by each participant, based on what they
364 perceived "tastes most like nothing." Tasteless solutions were one of either 25mM KCl /2.5mM
365 NaH CO3, 18.75mM KCl/1.875mM NaHCO3, 12.5mM KCl/1.25mM NaHCO3, 6.25mM
366 KCl/0.625mM NaHCO3, or 3.13mM KCl/0.313mM NaHCO3, dissolved in distilled water.

367 **Stimulus Delivery**

368 0.5 mL of milkshake was delivered into the mouth over 2s using an MRI-compatible gustometer
369 system. The gustometer system (*51*) is a portable device controlling 11 programmable BS-8000
370 syringe pumps (Braintree scientific, Braintree, Ma). Pumps are loaded with 60 mL syringes filled
371 with milkshake, which are infused into 25ft of Tygon beverage tubing (Saint-Gobain
372 Performance Plastics, Akron, OH) connected a Teflon gustatory manifold on the MRI headcoil.
373 The manifold consists of multiple channels that converge at a central point to allow delivery of a
374 liquid stimulus to the tongue tip.

375 **Preprocessing**

376 Neuroimaging data were preprocessed using SPM12 (Statistical Parametric Mapping, Wellcome
377 Department of Imaging Neuroscience, London, UK) and BioImage Suite (*52*). Participants'
378 functional images were corrected for geometric distortions resulting from susceptibility-induced
379 field inhomogeneities. The FieldMap toolbox in SPM12 was used to calculate static distortions
380 (*53*). Corrections were then made for both static distortions and changes in these distortions

381 resulting from head motion (*54*, *55*). Images were realigned, unwarped, and coregistered to each
382 participant's anatomical T1 image and then processed using a method combining segmentation,
383 bias correction, and spatial normalization (*56*). Functional images were slice-time corrected,
384 normalized to a standard MNI template, and smoothed using a 6 mm FWHM isotropic Gaussian
385 kernel. Normalized, motion-corrected images were further preprocessed using BioImage Suite.
386 These additional steps included regression of the mean time courses of global signal, CSF, and
387 white matter, in addition to removal of the linear trend and low-pass filtering.

388 **Construction of predictive networks**

389 We performed Connectome-based Predictive Modeling (CPM; *14*, *15*, *18*) to determine whether
390 task-based functional connectivity during milkshake receipt can predict individual differences in
391 anthropometric measurements. To accomplish this, we first used a whole-brain functional atlas
392 (*57*) to parcellate the brains of each subject into 268 nodes (i.e spatial ROIs) that maximize the
393 similarity of voxel-wise time courses within each node. 268x268 connectivity matrices for each
394 run were subsequently created in BioImage Suite by averaging the BOLD signal of each voxel
395 within nodes (*52*). Connectivity matrices were Fisher Transformed to convert the skewed
396 distribution of Pearson r (or Spearman rho) values to an approximately normal distribution.
397 Matrices were then averaged across runs to create a mean matrix for each subject, which were
398 then collapsed across subjects to create 268x268xN-subject matrices.

399 In the N-1 training set, CPM uses a linear regression (i.e. Pearson's r or Spearman's Rho) to
400 correlate each edge (i.e. connection) in each connectivity matrix to a behavioral measure of
401 interest. Each edge, as a result, is then associated with a particular p-value and the most relevant
402 edges are selected for further use via thresholding (P = 0.01). Edges that are positively correlated
403 with behavior constitute a "positive prediction network," while edges whose strengths are

404 negatively correlated with behavior constitute a "negative prediction network." Single-subject
405 summary values are then calculated by separately summing the edge-strengths of positive and
406 negative prediction networks (*15*). These positive and negative "network strengths" are used in a
407 linear model with behavior and applied prospectively to the left-out subject's network strengths
408 to generate predicted behavioral scores.

409 **Permutation Testing**

410 To determine the significance of the obtained correlations between observed and predicted
411 behavioral scores, we conducted 1000 repetitions of CPM using randomly shuffled observed
412 scores to generate predicted scores and networks. The 1000 correlation coefficients obtained
413 from permutation testing were used to comprise a null distribution against which the correlation
414 coefficients in the Results section were tested for significance. Final p-values were calculated by
415 determining the number of permutations, out of 1000, that generated correlation coefficients
416 larger than those reported in Results.

417 **Visualization**

418 Figures were constructed using BioImage Suite (*52*) and custom scripts in MATLAB® 2016b.
419 Anatomical locations were isolated using the Wake Forest PickAtlas Toolbox v. 3.0.5 (Wake
420 Forest University, Winston-Salem, NC, USA) in SPM12 and the Automated Anatomical
421 Labeling (AAL) atlas (*58*).

422

423 **Code Availability**

424 Matlab scripts to run the CPM analyses are available at
425 (https://www.nitrc.org/projects/bioimagesuite/). Visualization tools are available online through

BioImage Suite and accessible at (https://bisweb.yale.edu). Additional Matlab scripts for post-hoc analyses and visualization are available from the authors upon request.

Data Availability

The data used to support the findings of this study are available from the corresponding authors (M.C.F. and D.M.S.) upon reasonable request.

432 **References and Notes:**

433 1. O'Rahilly, S. & Farooqi, I. S. Human obesity: A heritable neurobehavioral disorder that is
434 highly sensitive to environmental conditions. *Diabetes* **57**, 2905–2910 (2008).
435
436 2. Frayling, T. M. *et al.* A common variant in the FTO gene is associated with body mass index
437 and predisposes to childhood and adult obesity. *Science* **316**, 889–894 (2007).
438
439 3. Scuteri, A. *et al.* Genome-wide association scan shows genetic variants in the FTO gene are
440 associated with obesity-related traits. *PLoS Genetics* **3**, 1200–1211 (2007).
441
442 4. Hess, M. E. *et al.* The fat mass and obesity associated gene (FTO) regulates activity of the
443 dopaminergic midbrain circuitry. *Nature Neuroscience* **16**, 1042–1048 (2013).
444
445 5. Smemo, S. *et al.* Obesity-associated variants within FTO form long-range functional
446 connections with IRX3. *Nature* **507**, 371–375 (2014).
447
448 6. Sevgi, M. *et al.* An obesity-predisposing variant of the FTO gene regulates D2R-dependent
449 reward learning. *Journal of Neuroscience* **35**, 12584–12592 (2015).
450
451 7. Loos, R. J. F. & Yeo, G. S. H. The bigger picture of FTO—the first GWAS-identified obesity
452 gene. *Nature Reviews Endocrinology* **10**, 51–61 (2014).
453

454 8. Locke, A. E. *et al.* Genetic studies of body mass index yield new insights for obesity biology.
455 *Nature* **518**, 197–206 (2015).
456
457 9. WHO, Physical Status: The Use and Interpretation of Anthropometry: Report of a World
458 Health Organization (WHO) Expert Committee. Geneva, Switzerland: World Health
459 Organization (1995).
460
461 10. Dudeja, V. *et al.* BMI does not accurately predict overweight in Asian Indians in Northern
462 India. *British Journal of Nutrition* **86**, 105–112 (2001).
463
464 11. Ode, J. J., Pivarnik, J. M., Reeves, M. J. & Knous, J. L. Body mass index as a predictor of
465 percent fat in college athletes and nonathletes. *Medicine & Science in Sports & Exercise* **39**,
466 403–409 (2007).
467
468 12. Kissebah, A. H. *et al.* Relation of body fat distribution to metabolic complications of obesity.
469 *The Journal of Clinical Endocrinology & Metabolism* **54**, 254–260 (1982).
470
471 13. Goodpaster, B. H. *et al.* Obesity, regional body fat distribution, and the metabolic syndrome
472 in older men and women. *Arch Intern Med* **165**, 777–783 (2005).
473
474 14. Finn, E. S. *et al.* Functional connectome fingerprinting: Identifying individuals using patterns
475 of brain connectivity. *Nature Neuroscience* **18**, 1664–1671 (2015).

15. Shen, X. *et al.* Using connectome-based predictive modeling to predict individual behavior from brain connectivity. *Nature Protocols* **12**, 506–518 (2017).

16. Hsu, W. T., Rosenberg, M. D., Scheinost, D., Constable, R. T. & Chun, M. M. Resting-state functional connectivity predicts neuroticism and extraversion in novel individuals. *Social Cognitive and Affective Neuroscience* **13**, 224–232 (2018).

17. Beaty, R. E. *et al.* Robust prediction of individual creative ability from brain functional connectivity. *Proceedings of the National Academy of Sciences* **115**, 1087–1092 (2018).

18. Rosenberg, M. D. *et al.* A neuromarker of sustained attention from whole-brain functional connectivity. *Nature Neuroscience* **19**, 165–171 (2016).

19. Greene, A. S., Gao, S., Scheinost, D. & Constable, R. T. Task-induced brain state manipulation improves prediction of individual traits. *Nature Communications* **9**, 2807 (2018).

20. Noble, S. *et al.* Influences on the test–retest reliability of functional connectivity MRI and its relationship with behavioral utility. *Cerebral Cortex* **27**, 5415–5429 (2017).

21. Satterthwaite, T. D. *et al.* An improved framework for confound regression and filtering for control of motion artifact in the preprocessing of resting-state functional connectivity data. *NeuroImage* **64**, 240–256 (2013).

499 22. Hodgson, K. *et al.* Shared genetic factors influence head motion during MRI and body mass
500 index. *Cerebral Cortex* **27**, 5539–5546 (2016).
501
502 23. Motamed, N. *et al.* The best obesity indices to discriminate type 2 diabetes mellitus.
503 *Metabolic Syndrome and Related Disorders* **14**, 249–253 (2016).
504
505 24. Bergman, R. N. *et al.* A better index of body adiposity. *Obesity* **19**, 1083–1089 (2011).
506
507 25. Ashwell, M., Gunn, P. & Gibson, S. Waist-to-height ratio is a better screening tool than waist
508 circumference and BMI for adult cardiometabolic risk factors: Systematic review and meta-
509 analysis. *Obesity Reviews* **13**, 275–286 (2012).
510
511 26. Seo, D. C., Choe, S. & Torabi, M. R. Is waist circumference ≥ 102/88 cm better than body
512 mass index ≥ 30 to predict hypertension and diabetes development regardless of gender, age
513 group, and race/ethnicity? Meta-analysis. *Preventive Medicine* **97**, 100–108 (2017).
514
515 27. Tanamas, S. K. *et al.* Quantifying the proportion of deaths due to body mass index- and waist
516 circumference-defined obesity: Mortality attributable to obesity. *Obesity* **24**, 735–742 (2016).
517
518 28. Dimitriadis, K. *et al.* Waist circumference compared with other obesity parameters as
519 determinants of coronary artery disease in essential hypertension: A 6-year follow-up study.
520 *Hypertension Research* **39**, 475–479 (2016).
521

522 29. Kurth, F. *et al.* Relationships between gray matter, body mass index, and waist circumference
523 in healthy adults. *Human Brain Mapping* **34**, 1737–1746 (2013).
524
525 30. Janowitz, D. *et al.* Association between waist circumference and gray matter volume in 2344
526 individuals from two adult community-based samples. *NeuroImage* **122**, 149–157 (2015).
527
528 31. Luo, S. *et al.* Abdominal fat is associated with a greater brain reward response to high-calorie
529 food cues in hispanic women. *Obesity* **21**, 2029–2036 (2013).
530
531 32. Green, E., Jacobson, A., Haase, L. & Murphy, C. Reduced nucleus accumbens and caudate
532 nucleus activation to a pleasant taste is associated with obesity in older adults. *Brain Research*
533 **1386**, 109–117 (2011).
534
535 33. Wallner-Liebmann, S. *et al.* Insulin and hippocampus activation in response to images of
536 high-calorie food in normal weight and obese adolescents. *Obesity* **18**, 1552–1557 (2010).
537
538 34. Janssen, I., Katzmarzyk, P. T. & Ross, R. Waist circumference and not body mass index
539 explains obesity-related health risk. *The American Journal of Clinical Nutrition* **79**, 379–384
540 (2004).
541
542 35. Jastreboff, A. M. *et al.* Neural correlates of stress- and food cue-induced food craving in
543 obesity: Association with insulin levels. *Diabetes Care* **36**, 394–402 (2013).
544

545 36. Noori, H. R., Cosa Linan, A. & Spanagel, R. Largely overlapping neuronal substrates of
546 reactivity to drug, gambling, food and sexual cues: A comprehensive meta-analysis. *European*
547 *Neuropsychopharmacology* **26**, 1419–1430 (2016).
548
549 37. Sun, X. *et al.* Basolateral amygdala response to food cues in the absence of hunger is
550 associated with weight gain susceptibility. *Journal of Neuroscience* **35**, 7964–7976 (2015).
551
552 38. Stice, E., Spoor, S., Bohon, C. & Small, D. M. Relation between obesity and blunted striatal
553 response to food is moderated by TaqIA A1 allele. *Science* **322**, 449–452 (2008).
554
555 39. Nguyen, Q. M., Srinivasan, S. R., Xu, J.-H., Chen, W. & Berenson, G. S. Distribution and
556 cardiovascular risk correlates of hemoglobin A1c in nondiabetic younger adults: The Bogalusa
557 Heart Study. *Metabolism* **57**, 1487–1492 (2008).
558
559 40. Vazquez, G., Duval, S., Jacobs, D. R. & Silventoinen, K. Comparison of body mass index,
560 waist circumference, and waist/hip ratio in predicting incident diabetes: A meta-analysis.
561 *Epidemiologic Reviews* **29**, 115–128 (2007).
562
563 41. Wang, Y., Rimm, E. B., Stampfer, M. J., Willett, W. C. & Hu, F. B. Comparison of
564 abdominal adiposity and overall obesity in predicting risk of type 2 diabetes among men. *The*
565 *American Journal of Clinical Nutrition* **81**, 555–563 (2005).
566
567

42. Woo, C. W., Chang, L. J., Lindquist, M. A. & Wager, T. D. Building better biomarkers: brain models in translational neuroimaging. *Nature Neuroscience* **20**, 365–377 (2017).

43. Scheinost, D. *et al.* Orbitofrontal cortex neurofeedback produces lasting changes in contamination anxiety and resting-state connectivity. *Translational Psychiatry* **3**, e250 (2013).

44. Koush, Y. *et al.* Learning control over emotion networks through connectivity-based neurofeedback. *Cerebral Cortex* **27**, 1193–1202 (2015).

45. Orlov, N. D. *et al.* Real-time fMRI neurofeedback to down-regulate superior temporal gyrus activity in patients with schizophrenia and auditory hallucinations: A proof-of-concept study. *Translational Psychiatry* **8**, 46 (2018).

46. Rosenberg, M. D. *et al.* Methylphenidate modulates functional network connectivity to enhance attention. *Journal of Neuroscience* **36**, 9547–9557 (2016).

47. Yip, S. W., Scheinost, D., Potenza, M. N. & Carroll, K. M. Connectome-based prediction of cocaine abstinence. *AJP* **176**, 156–164 (2019).

48. Shuster, A., Patlas, M., Pinthus, J. H. & Mourtzakis, M. The clinical importance of visceral adiposity: A critical review of methods for visceral adipose tissue analysis. *The British Journal of Radiology* **85**, 1–10 (2012).

590 49. Singh, B. Surrogate markers of insulin resistance: A review. *World Journal of Diabetes* **1**,
591 36–47 (2010).
592
593 50. Matthews, D. R. *et al.* Homeostasis model assessment: Insulin resistance and β-cell function
594 from fasting plasma glucose and insulin concentrations in man. *Diabetologia* **28**, 412-419
595 (1985).
596
597 51. Veldhuizen, M. G., Bender, G., Constable, R. T. & Small, D. M. Trying to detect taste in a
598 tasteless solution: Modulation of early gustatory cortex by attention to taste. *Chemical Senses* **32**,
599 569–581 (2007).
600
601 52. Joshi, A. *et al.* Unified framework for development, deployment and robust testing of
602 neuroimaging algorithms. *Neuroinformatics* **9**, 69–84 (2011).
603
604 53. Hutton, C., Deichmann, R., Turner, R., Andersson J., Combined correction for geometric
605 distortion and its interaction with head movement in fMRI. In *Proc. of the 12th Scientific*
606 *Meeting and Exhibition of the ISMRM* **12**, 1084 (2004).
607
608 54. Andersson, J. L. R., Hutton, C., Ashburner, J., Turner, R. & Friston, K. Modeling geometric
609 deformations in epi time series. *NeuroImage* **13**, 903–919 (2001).
610
611 55. Hutton, C. *et al.* Image distortion correction in fMRI: A quantitative evaluation. *NeuroImage*
612 **16**, 217–240 (2002).

613 56. Ashburner, J. & Friston, K. J. Unified segmentation. *NeuroImage* **26**, 839–851 (2005).

614

615 57. Shen, X., Tokoglu, F., Papademetris, X. & Constable, R. T. Groupwise whole-brain

616 parcellation from resting-state fMRI data for network node identification. *NeuroImage* **82**, 403–

617 415 (2013).

618

619 58. Lancaster, J. L. *et al.* Automated Talairach Atlas labels for functional brain mapping. *Human*

620 *Brain Mapping* **10**, 120–131 (2000).

621

622 **Acknowledgements:** We would like to thank Corey L Horien and Abigail Greene for their help

623 with data visualization. This work was supported by the National Institutes of Health training

624 grant T32NS041228 (M.C.F.); the Yale Medical School Fellowship (M.C.F.); the National

625 Institutes of Health R01 CA180030 (D.M.S.).

626 **Author Contributions:** Conceptualization, D.M.S. and M.C.F.; Investigation D.M.S and

627 M.C.F.; Software, R.T.C. and D.S.; Formal Analysis, M.C.F. and M.J.V.; Visualization, M.C.F.

628 and M.J.V.; Writing – Original Draft, M.C.F. and M.J.V.; Writing – Review and Editing, M.C.F.

629 and D.M.S.; Supervision, R.T.C., D.S., and D.M.S., Funding Acquisition, D.M.S.

630 **Competing Interests**: The authors declare no competing interests.

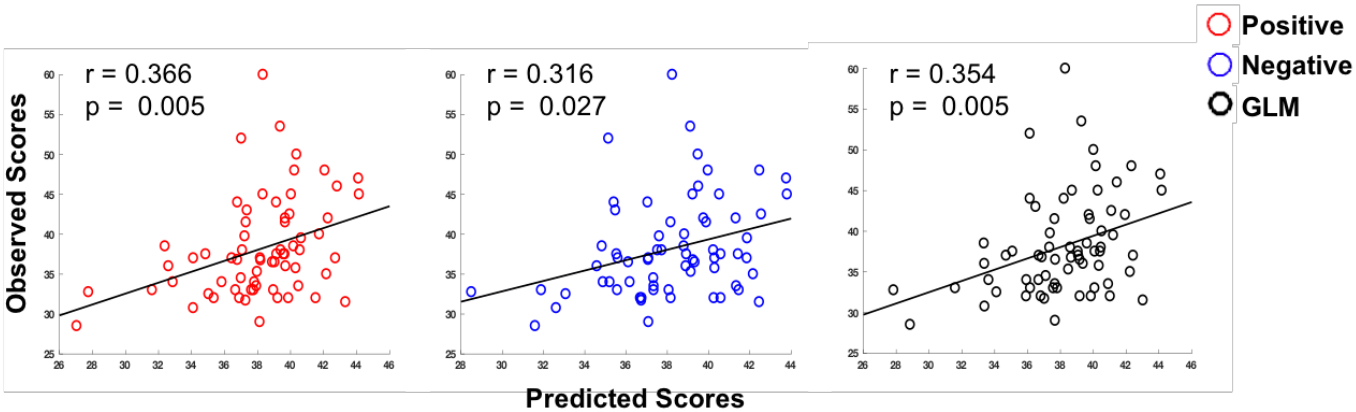

Fig. 1. Relationship Between Observed and Predicted Waist Circumference.

Scatterplots relating observed versus predicted waist circumference in positive, negative, and combined networks. Positive networks consist of edges that are positively correlated with behavior, while negative networks are constructed using edges that are negatively correlated with behavior. Combined networks are constructed using a general linear model (GLM). Overall, approximately 13% of the variance in a novel individual's waist circumference can be accounted for using CPM.

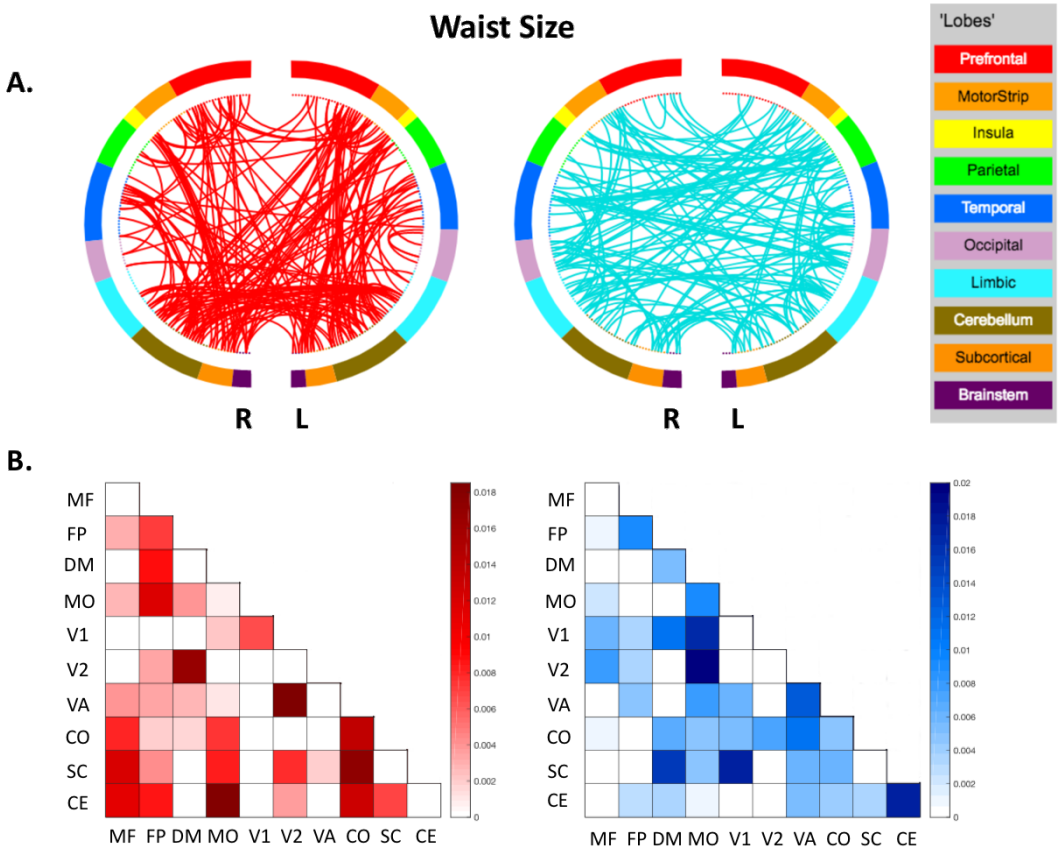

Fig. 2. Visualization of Positive and Negative Predictive Networks.

Representations of positive (red) and negative (blue) predictive networks in (**A**). Each semicircle is a different hemisphere of the brain. Connections represent edges between nodes, with nodes organized among ten macroscale regions. Matrices (**B**) show the proportion of positive versus negative edges shared between network pairs among ten canonical networks normalized for network size (MF: medial frontal; FP: frontoparietal; DM: default mode; MO: Motor; V1: visual 1; V2: visual 2; VA: visual association; CO: cingulo-opercular; SC: subcortical; CE: cerebellar).

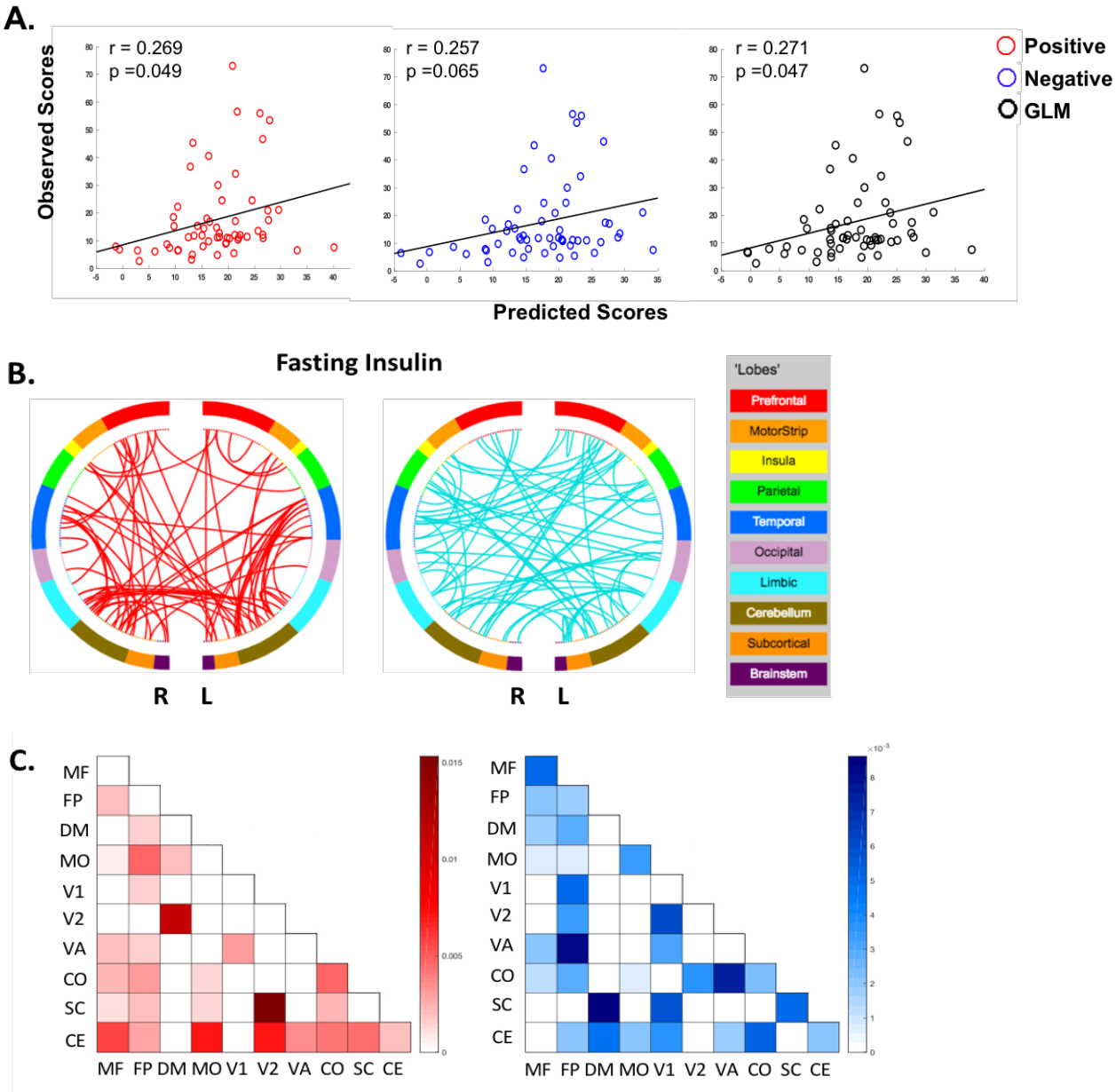

Fig. 3. Exploratory Analysis of Fasting Insulin

CPM predicts fasting insulin levels (**A**). Positive and negative predictive networks are shown as hemisphere plots in (**B**). Notably, the number of positive and negative edges are highest among cerebellar and frontoparietal regions and the rest of the brain (**C**).

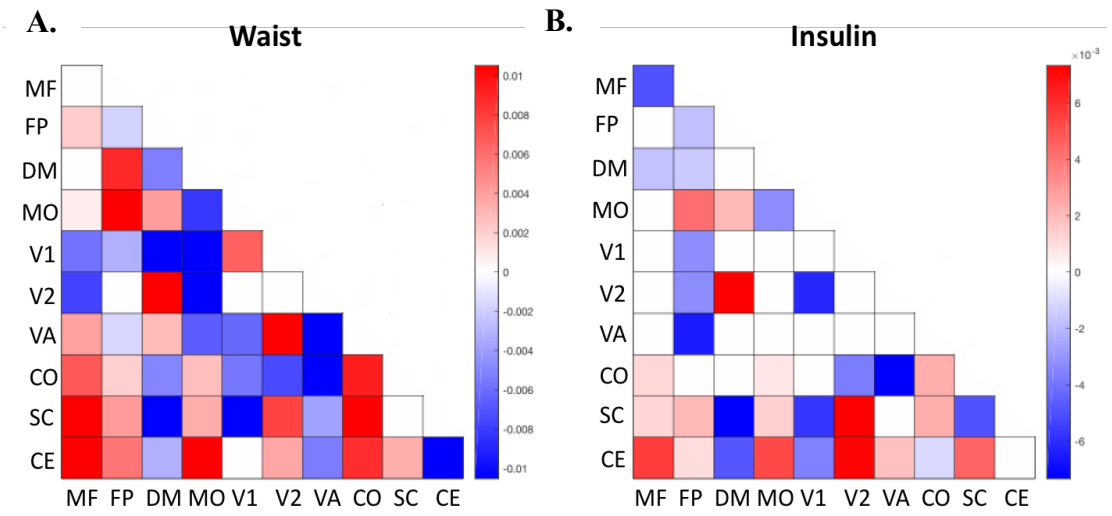

Fig. 4. Difference Matrices of Waist Circumference and Insulin

Matrices express the polarity in the number of positive versus negative edges between canonical networks adjusted for network size. For example, (**A**) shows more edges in the positive network exist between cerebellar and medial frontal nodes, while more edges in the negative network exist for cerebellar-cerebellar connections. Taken together, (**A**) and (**B**) demonstrate the greatest degree of similarity in connectivity patterns of cerebellar and subcortical networks in waist circumference and fasting insulin CPMs.

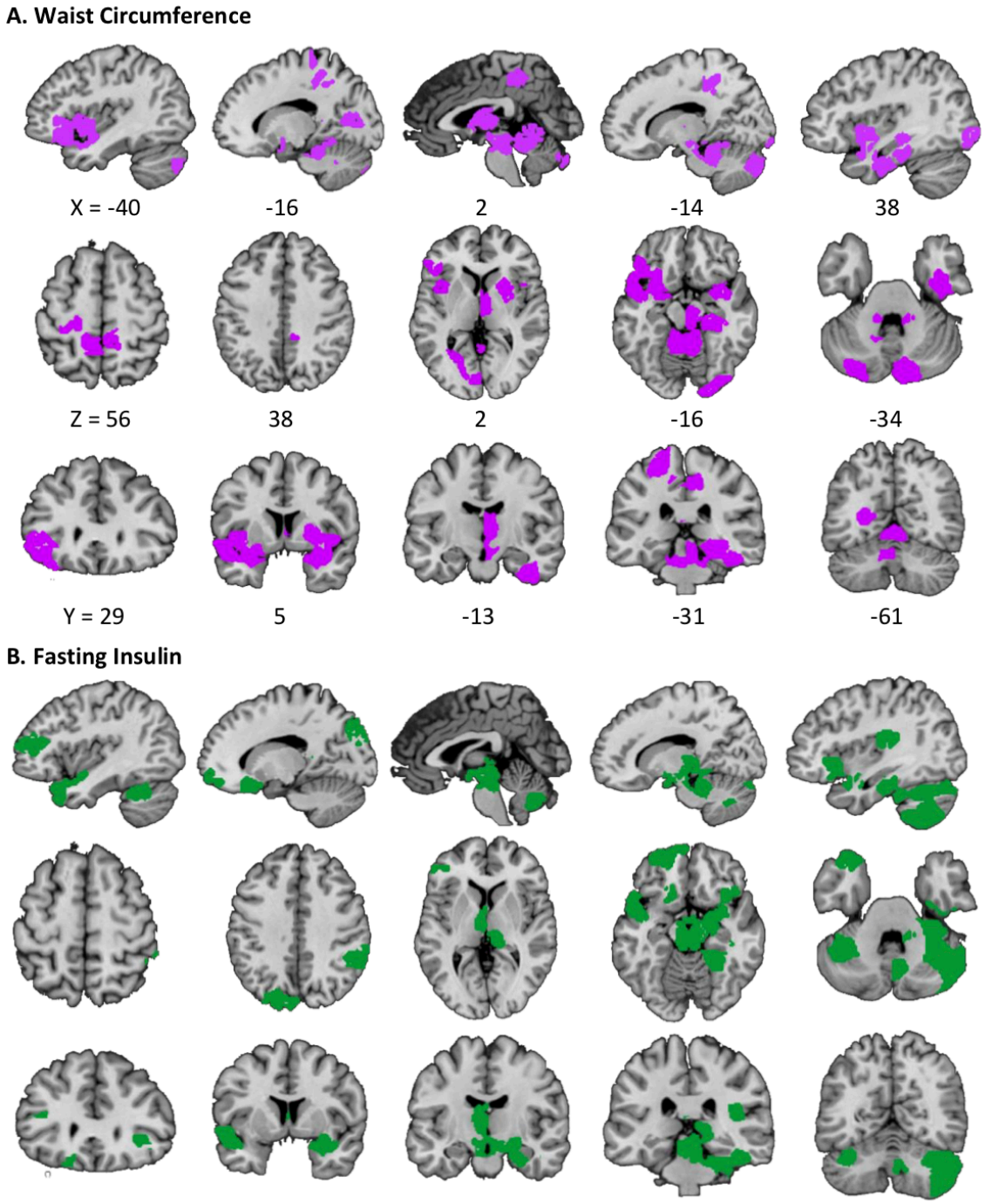

Fig. 5. Top 10% High-Degree Nodes for Waist Circumference and Fasting Insulin CPMs

Top 10% high-degree nodes (27 nodes total) for waist circumference (**A**) encompass networks spanning the whole brain and include nodes varying in degree from 21 to 7. (**B**) The CPM for fasting insulin is similarly encompassing, with nodes varying in degree from 11 to 3.

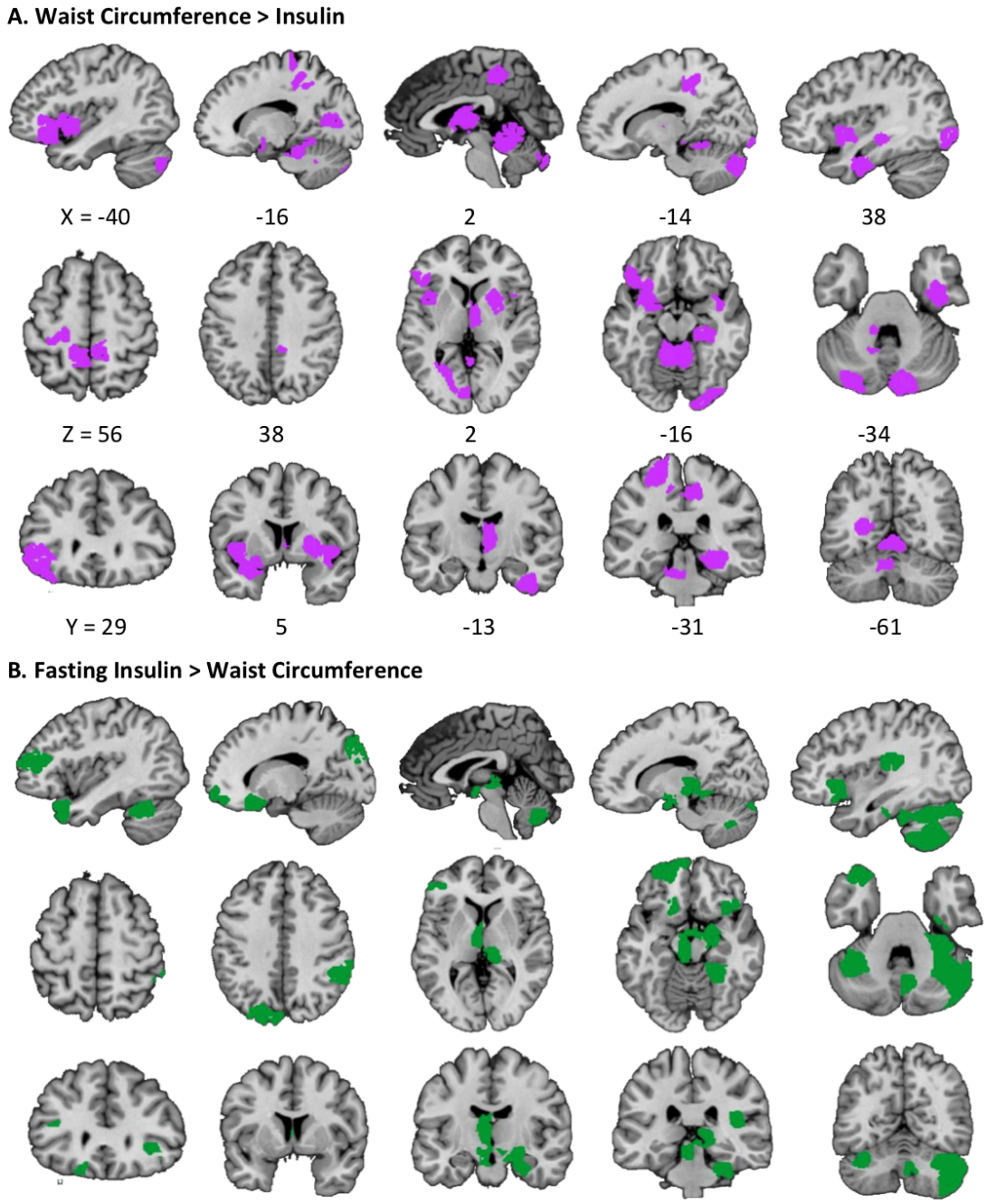

Fig. 6. Difference of Top 10% Nodes between Waist Circumference and Fasting Insulin CPMs

(**A**) High-degree nodes (top 10%) participating in the waist circumference CPM but not the fasting insulin CPM (**B**) Nodes in the top 10% participating in the fasting insulin CPM but not the waist circumference CPM.

Table 1. Top 10% High-Degree Nodes in the Waist Circumference Network.

Degree	Node	Region	MNI Coordinates	AAI Label
21	172	L-Parietal	23.5, -31.6, 63.6	Postcentral gyrus
20	228	L-Limbic	-26.8, 2.4, -18.7	Left Amygdala
19	244	L-Cerebellum	-6.5, -50.2, -11.4	Left lobule IV,V Cerebellum
15	124	R-Subcortical	26.6, 6.3, 0.1	Right Putamen
15	59	R-Temporal	43.4, -26.5, -24.6	Right Fusiform
13	226	L-Limbic	-8.8, -42.6, 50.1	Left Midcingulate Area
12	169	L-Insula	-38.7, 8.1, -4.8	Left Insula
12	132	R-Brainstem	6.3, -24.9, -17.5	N/A (Midbrain)
10	255	L-Cerebellum	-6.6, -54.7, -26.3	N/A (Cerebellum)
9	153	L-Prefrontal	-32, 20.5, -16	Left Inferior Frontal Gyrus, Pars Orbitalis
8	251	L-Cerebellum	-10.3, -37.7, -25.1	Left Lobule III of Cerebellum
8	227	L-Limbic	-7.5, -42.1, 13.3	Left Posterior Cingulate Gyrus
8	151	L-Prefrontal	-46.2, 28.2, -7.1	Left Inferior Frontal Gyrus, Pars Orbitalis
8	111	R-Cerebellum	11.7, -84.1, -34.6	Right crus II of Cerebellum
8	101	R-Cerebellum	6.1, -50.7, -12.3	Lobule IV, V of Vermis
8	34	R-Insula	41.8, 5, -7.6	Right Insula
7	242	L-Cerebellum	-30.2, -80.2, -40.3	Left Crus II of Cerebellum
7	216	L-Occipital	-22.1, -66.7, 7.4	Left Calcarine Sulcus
7	215	L-Occipital	-6, -81.2, 12.2	Left Calcarine Sulcus
7	188	L-Temporal	-49.7, 6.4, -15.2	Left Superior Temporal Pole
7	128	R-Subcortical	5.5, -9.7, 5.2	Right Thalamus
7	103	R-Cerebellum	13.7, -40.1, -25.4	Right Lobule III of Cerebellum
7	95	R-Limbic	28, -28.4, -13.7	Right Parahippocampal Gyrus

7	92	R-Limbic	31.2, 3.7, -21.6	Right Superior Temporal Pole
7	91	R-Limbic	8.3, -39.9, 48.1	Right Midcingulate Area
7	81	R-Occipital	31.2, -91.8, -10.8	Right Inferior Occipital Lobe
7	58	R-Temporal	40.3, -11.3, -35.8	Right Fusiform Gyrus

Table 2. Top 10% High-Degree Nodes in the Fasting Insulin Network.

Degree	Node	Region	MNI Coordinates	AAL Label
11	238	L-Cerebellum	-37, -52.9, -31.1	Left Crus I of Cerebellum
8	186	L-Temporal	-34.6, 18.6, -32.2	Left Superior Temporal Pole
7	227	L-Limbic	-7.5, -42.1, 13.3	Left Posterior Cingulate Gyrus
7	59	R-Temporal	43.4, -26.5, -24.6	Right Fusiform
6	116	R-Cerebellum	41.9, -64, -49.2	Right Lobule VIIB of Cerebellum
5	103	R=Cerebellum	13.7, -40.1, -25.4	Right Lobule III of Cerebellum
5	102	R-Cerebellum	39.1, -74.9, -29.7	Right Crus I of Cerebellum
5	92	R-Limbic	31.2, 3.7, -21.6	Right Superior Temporal Pole
4	265	L-Brainstem	-5, -21.5, -15.8	N/A (Midbrain)
4	263	L-Subcortical	-4.9, -10.3, 5.8	Left Thalamus
4	208	L-Occipital	-16.8, -84.9, 33	Left Cuneus
4	188	L-Temporal	-49.7, 6.4, -15.2	Left Superior Temporal Pole
4	154	L-Prefrontal	-43, 42, 11	Left Inferior Frontal Gyrus Pars Triangularis
4	139	L-Prefrontal	-18.2, 57, -14.3	Left Superior Frontal Gyrus, Orbital part
4	99	R-Limbic	19.3, -7.7, -14.8	Right Hippocampus
4	36	R-Insula	37.5, 21.1, -10.1	Right Inferior Frontal Gyrus, Orbital part
3	255	L-Cerebellum	-6.6, -54.7, -26.3	N/A (Cerebellum)
3	254	L-Cerebellum	-21.2, -53.4, -23.6	Left Lobule VI of Cerebellum
3	253	L-Cerebellum	-26.3, -69.5, -30.6	Left Crus I of Cerebellum
3	252	L-Cerebellum	-46.4, -46.8, -42.9	Left Crus II of Cerebellum
3	251	L-Cerebellum	-10.3, -37.7, -25.1	Left lobule III of Cerebellum

3	246	L-Cerebellum	-42.6, -63.7, -46.3	Left Crus II of Cerebellum
3	242	L-Cerebellum	-30.2, -80.2, -40.3	Left Crus II of Cerebellum
3	202	L-Temporal	-30, -5.8, -40.9	Left Fusiform Gyrus
3	163	L-MotorStrip	-57, -3.4, 6.8	Left Superior Temporal Gyrus
3	135	L-Prefrontal	-18.2, 19, -21	Left Inferior Frontal Gyrus, Pars Orbitalis
3	132	R-Brainstem	6.3, -24.9, -17.5	N/A (Midbrain)